

# Adaptation of Wallace’s Approach to the Specific Heat of Elemental Solids with Significant Intrinsic Anharmonicity, Particularly the Light Actinide Metals

Christopher A. Mizzi, W. Adam Phelan, Matthew S. Cook, Greta L. Chappell, Paul H. Tobash, David C. Arellano, Derek V. Prada, Boris Maiorov, and Neil Harrison  
*Los Alamos National Laboratory, Los Alamos, NM 87545*

(Dated: December 12, 2024)

The quasiharmonic approximation is the most common method for modeling the specific heat of solids; however, it fails to capture the effects of intrinsic anharmonicity in phonons. In this study, we introduce the “elastic softening approximation,” an alternative approach to modelling intrinsic anharmonic effects on thermodynamic quantities which is grounded in Wallace’s thermodynamic framework (*Thermodynamics of Crystals*, 1972) and focused on tracking entropy changes due to the continuous softening of phonons as a function of temperature. A key finding of our study is a direct correlation between Poisson’s ratio and the differential rate of phonon softening at finite frequencies, compared to lower frequencies relevant to elastic moduli measurements. We observe that elemental solids such as  $\alpha$ -Be, diamond, Al, Cu, In, W, Au, and Pb, which span a wide range of Poisson’s ratios and exhibit varying degrees of intrinsic anharmonicity, consistently follow this trend. When applied to  $\alpha$ -U,  $\alpha$ -Pu, and  $\delta$ -Pu, our method reveals unusually large anharmonic phonon contributions at elevated temperatures across all three light actinide metals. These findings are attributed to the unique combination of enhanced covalency and softer elastic moduli inherent in the actinides, potentially influenced by their  $5f$ -electron bonding.

## INTRODUCTION

To understand how materials behave under extreme conditions, it is crucial to know how entropy changes with temperature [1–4]. One method to assess the predictability of phonons involves the quasiharmonic approximation [5], which extends the harmonic model to consider the impact of thermal expansion and contraction against a bulk modulus. The quasiharmonic approach models the specific heat of phonons,  $C_{p,\text{ph}}(T)$ , as a function of temperature at constant pressure, starting with the specific heat at constant volume,  $C_{v,\text{ph}}(T)$ , calculated from the phonon density of states as in a harmonic crystal [6]. It then incorporates a term that factors in thermal expansivity and the isothermal bulk modulus [5]. Such an approach proves to be especially useful in systems exhibiting small shifts in phonon frequencies with temperature attributable to intrinsic anharmonicity, such as solid Al [7].

Problems arise with the quasiharmonic approximation when intrinsic anharmonicity effects become significant, as these effects are neglected in this approach. By “intrinsic anharmonicity,” we refer to systems where notable changes in phonon frequencies occur under conditions of near constant volume [5, 8]. While intrinsic anharmonic effects become important in most solids at sufficiently high temperatures, it dominates over a larger temperature range in materials that simultaneously exhibit negative thermal expansion and phonon frequency softening with increasing temperature [9]. Such effects are especially pronounced in the actinide metal

$\delta$ -Pu [10–12]. In addition to exhibiting a negative thermal expansivity at high temperatures [13–15]—a rare trait for an elemental solid—it also exhibits an anomalously large phonon softening with increasing temperature, as documented by elastic moduli measurements [16] and temperature-dependent neutron scattering measurements of the phonon density of states [17].

In this paper, we introduce an alternative to the quasiharmonic approximation for modeling the specific heat of elemental solids at high temperatures, which we term the ‘elastic softening approximation.’ Based on the approach of Wallace [18], this method is designed to address the limitations of the quasiharmonic approximation and considers the effect of continuous softening of phonon frequencies on the entropy as a function of temperature [8, 18, 19]. Specifically, it captures significant contributions from intrinsic anharmonic phonon effects involving changes in phonon frequencies that are unrelated to thermal expansivity, as observed in  $\delta$ -Pu [16, 17].

We first test our approach on a variety of regular elemental solids with different crystal structures, namely  $\alpha$ -Be, diamond (C), Al, Cu, In, W, Au, and Pb. To fully capture the phonon contribution to specific heat at high temperatures, we introduce what we refer to as a differential softening parameter,  $\eta$ . This parameter accounts for the differences in the rate of phonon softening at finite frequencies compared to the vanishing frequency limit, which is relevant to elastic moduli measurements. In the few systems where the phonon density of states has been measured at multiple temperatures [7, 17, 20–22], we find that  $\eta$  accurately predicts the softening of

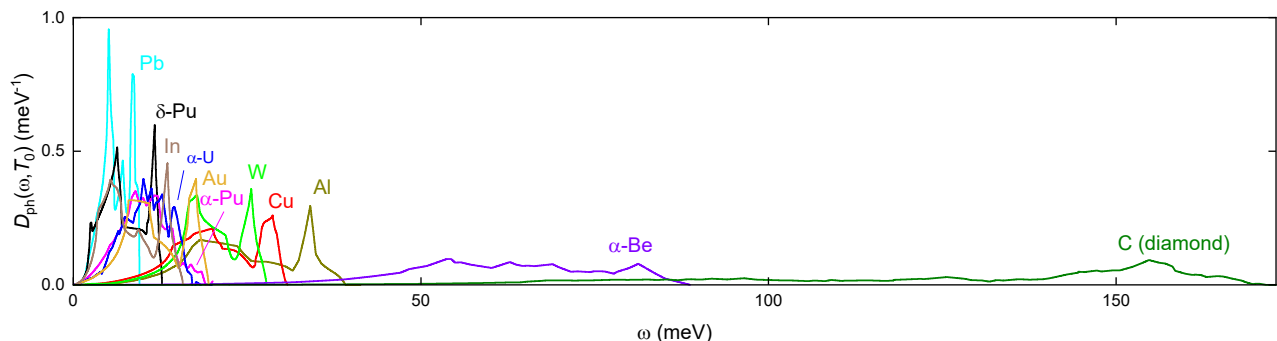


FIG. 1: The phonon density of states,  $D_{\text{ph}}(\omega, T_0)$ , measured at temperature  $T_0$  for the elemental solids  $\alpha$ -Be [36, 37], diamond [38], Al [39], Cu [40], In [41], W [41], Au [42], Pb [43],  $\alpha$ -U [44],  $\alpha$ -Pu [45], and  $\delta$ -Pu [46]. Values for  $T_0$  are given in Table I.

prominent features in the phonon density of states.

We also find that  $\eta$  is closely correlated with Poisson's ratio [23–25], suggesting a link between  $\eta$  and bonding. A larger  $\eta$  (indicating increased phonon softening at finite frequencies relative to ultrasound measurements) is linked to brittleness and more covalent bonding character. Conversely, a smaller  $\eta$  (indicating suppressed softening at finite frequencies) is associated with ductility and more metallic bonding character.

We observe that the actinide metals  $\alpha$ -U,  $\alpha$ -Pu, and  $\delta$ -Pu follow the same trend as other solids, once we account for their anomalous electronic contribution [26] to the specific heat at low temperatures. However, because the phonon softening in these actinides is much more dramatic than in other elemental solids, their intrinsic anharmonic contribution to the total specific heat is anomalously large, especially in  $\delta$ -Pu [10, 27–31].

## APPROXIMATIONS TO THE SPECIFIC HEAT

The phonon contribution to the specific heat  $C_{v,p,\text{ph}}(T)$  is related to the phononic entropy  $S_{\text{ph}}(T)$  via [32]

$$C_{v,p,\text{ph}}(T) = T \left. \frac{\partial S_{\text{ph}}(T)}{\partial T} \right|_{v,p}, \quad (1)$$

where  $T$  is temperature and the subscripts  $v$  and  $p$  refer to constant volume and constant pressure conditions, respectively.

While it is sometimes possible to achieve exceptionally good fits to the specific heat and other thermodynamic quantities using methods based on the Debye or Einstein models [6], particularly for modeling the equation of state [2, 33–35], such methods often require multiple adjustable parameters. This reliance on adjustable parameters can obscure the underlying physics we seek to investigate. To gain deeper insight into the limitations or advantages of a given approximation to the specific heat in relation to anharmonic phonon effects, we desire to utilize the measured phonon density of states, as depicted

in Fig. 1 [36–46], to determine the phonon contribution to the specific heat.

## Harmonic and Quasiharmonic Approximations to Phononic Entropy

The harmonic approximation (HA) models the phonon contribution to the specific heat at constant volume,  $C_{v,\text{ph}}^{\text{HA}}(T)$ , by assuming that the phonon frequencies,  $\omega$ , have no temperature dependence. Under this assumption, the phonon density of states,  $D_{\text{ph}}$ , is temperature independent [*i.e.*,  $D_{\text{ph}}(\omega, T) = D_{\text{ph}}(\omega, T_0)$  where  $T_0$  denotes the temperature at which the phonon density of states is measured, often around 300 K (see Table I)]. Temperature is assumed only to affect the phonon contribution to entropy via thermal occupancy. The phononic entropy can then be calculated from the phonon density of states using [5, 19]

$$S_{\text{ph}}(T) = R \int_0^\infty D_{\text{ph}}(\omega, T_0) \times [(n_{\text{BE}} + 1) \ln(n_{\text{BE}} + 1) - n_{\text{BE}} \ln(n_{\text{BE}})] d\omega, \quad (2)$$

where

$$n_{\text{BE}} = \left( e^{\frac{\hbar\omega}{k_{\text{B}}T}} - 1 \right)^{-1}$$

is the Bose-Einstein distribution function, and  $R = N_{\text{A}}k_{\text{B}}$  is the gas constant. Within this approximation,  $C_{v,\text{ph}}^{\text{HA}}(T)$  is found by performing the integration in Equation 2 using  $D_{\text{ph}}(\omega, T_0)$  and substituting this phonon contribution to entropy into Equation 1.

The quasiharmonic approximation (QHA) improves upon the HA by considering the effects of a temperature-dependent volume on the phonon contribution to the heat capacity. In QHA treatments, the lattice is modeled as uniformly expanding and contracting against a bulk modulus [5]. The phonon contribution to the heat capacity at constant pressure within the QHA,  $C_{p,\text{ph}}^{\text{QHA}}(T)$ , is then estimated as the sum of the HA contribution at

constant volume and a term describing the effects of the temperature-dependent volume changes,

$$C_{p,\text{ph}}^{\text{QHA}}(T) \approx C_{v,\text{ph}}^{\text{HA}}(T) + V(T)\alpha_v^2(T)B_T(T)T, \quad (3)$$

where  $V(T)$  is the molar volume,  $\alpha_v(T)$  the thermal expansivity, and  $B_T(T)$  the isothermal bulk modulus. The temperature-dependences of these quantities is nearly always neglected [5].

### Elastic Softening Approximation to Phononic Entropy

Since contributions of the form  $\frac{\partial\omega}{\partial V}|_T$  are included in the QHA [5], this treatment implicitly allows for phonon frequencies to vary with temperature through their dependence on volume. However, the QHA does not treat the temperature dependence of phonon frequencies [9],  $\frac{\partial\omega}{\partial T}|_V$ , caused by intrinsic anharmonicity [5, 8]. Intrinsic anharmonicity arises from a number of sources, including phonon-phonon and electron-phonon interactions [5]. It can be substantial in many systems at high temperatures [47] and pressures [8], and is expected to be dominant in systems with near zero thermal expansivity [9]. However, the treatment of intrinsic anharmonicity is still an open question.

One compelling approach to intrinsic anharmonicity was put forth by Wallace [18] who showed that, to first order, anharmonic phonon contributions to the entropy can be incorporated by utilizing experimental temperature-dependent phonon frequencies in the evaluation of Equation 2. Therefore, by replacing  $D_{\text{ph}}(\omega, T_0)$  with  $D_{\text{ph}}(\omega, T)$  and performing the integration in Equation 2, in principle, one can calculate  $C_{p,\text{ph}}(T)$  using Equation 1 over any desired parameter space provided experimental values of  $D_{\text{ph}}(\omega, T)$  are known. Note, we focus on the heat capacity at constant pressure because this is often the most experimentally accessible quantity. In practice, widespread application of Wallace's method is constrained by the limited availability of  $D_{\text{ph}}(\omega, T)$  data, often only available for a select range of temperatures and materials.

Without measurements of the entire density of states over a wide temperature range, the challenge is then to figure out ways to approximate the temperature dependence of the phonon frequencies. To this end, we propose our elastic softening approximation (ESA), which assumes that the temperature-dependence of phonon frequencies can be quantified by the factor  $\beta_p(T)$ . This factor is defined such that  $\beta_p(T) = \omega(T)/\omega(T_0)$ , where  $\omega$  refers to a reference frequency in the phonon spectrum, with  $\beta_p(T_0) = 1$  at the reference temperature  $T_0$ . In this approximation, the phonon density of states undergoes a continuous temperature-dependent rescaling relative to the phonon density of states at  $T_0$ , as represented by the

equation:

$$D_{\text{ph}}(\omega, T) \approx \beta_p^{-1}(T)D_{\text{ph}}(\omega\beta_p^{-1}(T), T_0), \quad (4)$$

resulting in a shift of the phonon density of states to lower frequencies at higher temperatures, while maintaining the total number of phonon states.

The impact of temperature-dependent phonon frequency changes on entropy is a critical initial consideration prior to deriving other thermodynamic quantities, such as the specific heat [8, 18, 19]. We do this by substituting  $D_{\text{ph}}(\omega, T)$  in Equation 4 for  $D_{\text{ph}}(\omega, T_0)$  in Equation 2 and then determining the specific heat using Equation 1.

This approach is consistent with Wallace's approach as shown by introducing a variable change:  $\omega' = \beta_p^{-1}(T)\omega$ . This leads to an altered expression for the entropy:

$$S_{p,\text{ph}}^{\text{ESA}}(T) = R \int_0^\infty D_{\text{ph}}(\omega', T_0) \times [(n'_{\text{BE}} + 1) \ln(n'_{\text{BE}} + 1) - n'_{\text{BE}} \ln(n'_{\text{BE}})] d\omega', \quad (5)$$

resembling Equation 2, but where the Bose-Einstein distribution function is modified to

$$n'_{\text{BE}} = \left( e^{\frac{\hbar\omega'\beta_p(T)}{k_B T}} - 1 \right)^{-1}.$$

At  $T = T_0$ , where  $\beta_p(T = T_0) = 1$ , the entropy described by Equation 5 aligns with the harmonic approximation at temperature  $T_0$ . We show consistency with Wallace's approach explicitly by considering the frequency shift as a small perturbation:  $\delta\omega \approx \omega(\beta_p(T) - 1)$ . Upon substituting  $\beta_p(T) \approx 1 + \delta\omega/\omega$  into Equation (5), we obtain:

$$S_{p,\text{ph}}^{\text{ESA}}(T) \approx S_{v,\text{ph}}^{\text{HA}}(T) - \delta\omega \times N_A \int_0^\infty D_{\text{ph}}(\omega, T_0) \frac{\partial n_{\text{BE}}}{\partial T} d\omega, \quad (6)$$

which aligns with Wallace's expression for the anharmonic phonon contribution [8, 18]. The negative  $\delta\omega$  at high temperatures indicates that phonon softening invariably results in an increase in entropy.

The modified form of the Bose-Einstein distribution function in Equation 5 also implies that the effect of  $\beta_p(T)$  in our elastic softening approximation is to rescale  $S_{\text{ph}}(T)$  in temperature, so that  $S_{p,\text{ph}}^{\text{ESA}}(T) = S_{\text{ph}}(T/\beta_p(T))$ . Taking the derivative, we obtain

$$C_{p,\text{ph}}^{\text{ESA}}(T) = \left( \beta_p^{-1}(T) + T \frac{\partial\beta_p^{-1}(T)}{\partial T} \right) C_{v,\text{ph}}^{\text{HA}} \left( \frac{T}{\beta_p(T)} \right). \quad (7)$$

The terms  $\beta_p^{-1}(T)$  and  $\frac{\partial\beta_p^{-1}(T)}{\partial T}$  in our model cause the specific heat at high temperatures to exceed the Dulong-Petit limit, a phenomenon also observed in the quasi-harmonic approximation (*i.e.*, the second term on the right-hand-side of Equation 3 is always positive).

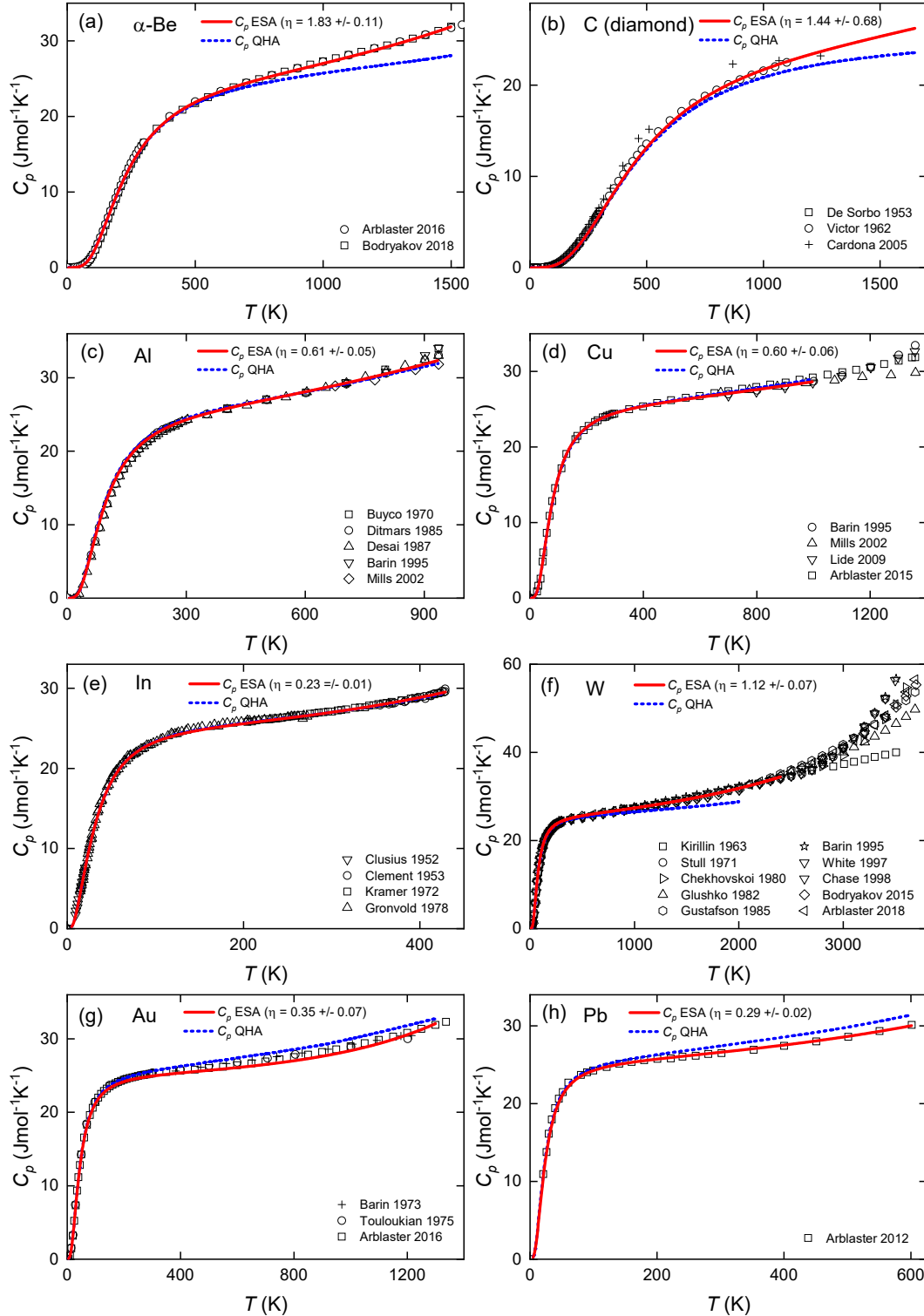


FIG. 2: Specific heat data (represented by symbols) for  $\alpha$ -Be (a), C (diamond) (b), Al (c), Cu (d), In (e), W (f), Au (g), and Pb (h) from various sources [49–77], as indicated. The dotted blue lines represent  $C_p^{\text{QHA}}(T)$  calculated assuming the quasi-harmonic approximation (QHA) using Equation 15. The solid red lines represent  $C_p^{\text{ESA}}(T)$  calculated assuming the elastic softening approximation (ESA) using Equation 17.

element	$T_0$ (K)	$V(T_0)$ ( $\text{cm}^3\text{mol}^{-1}$ )	$B_T(T_0)$	$\gamma_{\text{el}}$ ( $\text{mJmol}^{-1}\text{K}^{-2}$ )	$\eta$ (GPa)	$\nu(T \rightarrow 0)$
$\alpha$ -Be	300	4.851	107.4	0.17	$1.83 \pm 0.11$	0.042
C (diamond)	10	3.416	444.2	0.00	$1.44 \pm 0.68$	0.070
Al	300	10.002	72.7	1.26	$0.61 \pm 0.05$	0.335
Cu	80	7.044	140.3	0.69	$0.60 \pm 0.06$	0.340
In	77	15.469	45.7	1.66	$0.23 \pm 0.01$	0.420
W	298	9.551	307.2	1.01	$1.12 \pm 0.07$	0.279
Au	300	10.216	172.3	0.69	$0.35 \pm 0.07$	0.424
Pb	300	18.273	41.6	2.93	$0.29 \pm 0.02$	0.393
$\alpha$ -U	300	12.492	121.6	9.14	$1.17 \pm 0.20$	0.212
$\alpha$ -Pu	300	12.307	48.8	17	$1.45 \pm 0.20$	0.179
$\delta$ -Pu	300	14.892	30.6	64	$0.97 \pm 0.12$	0.273

TABLE I: Values of temperature  $T_0$  for each element at which the phonon density of states was measured (see Fig.1), along with the values of molar volume  $V(T_0)$ , and the isothermal bulk modulus  $B_T(T_0)$  at this temperature. The table also includes the Sommerfeld coefficient for each elemental solid, the obtained values of  $\eta$ , and the low-temperature Poisson's ratio  $\nu$  (determined from the data in Fig. 3). For  $\delta$ -Pu,  $V(T_0)$  corresponds to samples in which the  $\delta$  phase was stabilized by substituting 2 atomic percent of the Pu sites with Ga [15].

### Estimating Phonon Frequency Changes from Elastic Moduli

Within the ESA outlined above, the treatment of intrinsic anharmonicity amounts to finding a suitable method to quantify  $\beta_p(T)$ . We accomplish this by initially considering the elastic moduli, which are second derivatives of free energy with respect to strain [48]. Polycrystals with equiaxial distributions of grain orientation (the scope of this work) possess two independent elastic moduli, taken here to be the adiabatic longitudinal  $L_S(T)$  and shear  $G_S(T)$  elastic moduli. The former is related to the bulk and shear moduli via  $L_S(T) = B_S(T) + 4G_S(T)/3$ . Each of these isotropic moduli possess distinct temperature-dependences which, in the absence of phase transitions, describe the evolution of phonon frequencies with temperature in the limit  $\omega \rightarrow 0$  [48].

More explicitly, the above elastic moduli can be recast as sound velocities which are the gradient of the acoustic branches of the phonon dispersion in the long-wavelength limit. The two elastic moduli considered in this work are related to the longitudinal,  $c_{\text{long}}(T)$ , and transverse,  $c_{\text{tran}}(T)$ , sound velocities according to  $c_{\text{long}}(T) = \sqrt{L_S(T)/\rho(T)}$  and  $c_{\text{tran}}(T) = \sqrt{G_S(T)/\rho(T)}$ , where  $\rho(T)$  is the temperature-dependent density. Relative changes in these sound velocities with temperature from some reference temperature  $T_0$  are then given by:

$$\frac{c_{\text{long}}(T)}{c_{\text{long}}(T_0)} = \sqrt{\frac{L_S(T)\rho(T_0)}{L_S(T_0)\rho(T)}}, \quad (8)$$

$$\frac{c_{\text{tran}}(T)}{c_{\text{tran}}(T_0)} = \sqrt{\frac{G_S(T)\rho(T_0)}{G_S(T_0)\rho(T)}}. \quad (9)$$

Combining the definition of sound velocities in the  $\omega \rightarrow 0$  limit ( $\omega = ck$ ) with the definition of the elastic softening

parameter introduced above ( $\beta_p(T) = \omega(T)/\omega(T_0)$ ), the relative change in sound velocities with temperature will scale as:

$$\frac{c_{\text{long}}(T)}{c_{\text{long}}(T_0)} = \beta_{p,\text{long}}(T) \frac{k(T_0)}{k(T)}, \quad (10)$$

$$\frac{c_{\text{tran}}(T)}{c_{\text{tran}}(T_0)} = \beta_{p,\text{tran}}(T) \frac{k(T_0)}{k(T)}. \quad (11)$$

Here,  $k(T_0)/k(T)$  adjusts for the temperature dependence of the reciprocal lattice size, with  $k(T) \propto 1/\sqrt[3]{V(T)}$ .

Combining Equations 8 and 10, and also Equations 9 and 11, yields:

$$\beta_{p,\text{long}}(T) = \left(\frac{L_S(T)}{L_S(T_0)}\right)^{\frac{1}{2}} \left(\frac{V(T)}{V(T_0)}\right)^{\frac{1}{6}}, \quad (12)$$

$$\beta_{p,\text{tran}}(T) = \left(\frac{G_S(T)}{G_S(T_0)}\right)^{\frac{1}{2}} \left(\frac{V(T)}{V(T_0)}\right)^{\frac{1}{6}}. \quad (13)$$

These equations describe the softening of the longitudinal and transverse acoustic components of the phonon density of states with temperature, based on elastic moduli.

Since the experimental phonon density of states often lacks separation into these components, we use a weighted average of Equations 12 and 13 which accounts for the number of longitudinal acoustic and transverse acoustic phonon modes:

$$\beta_p^{-1}(T) \approx \left(\frac{1}{3} \left(\frac{L_S(T_0)}{L_S(T)}\right)^{\frac{1}{2}} + \frac{2}{3} \left(\frac{G_S(T_0)}{G_S(T)}\right)^{\frac{1}{2}}\right)^\eta \left(\frac{V(T)}{V(T_0)}\right)^{-\frac{1}{6}}. \quad (14)$$

Note, this expression will be dominated by contributions from  $G_S(T)$ . Our reason for taking the mean of the reciprocal  $\beta_p^{-1}(T)$ , as opposed to  $\beta_p(T)$ , is that it is the reciprocal quantity that scales the phonon density of states in Equation 4.

The changes in phonon frequency with temperature described by Equations 12 - 14 strictly apply in the limit  $\omega \rightarrow 0$  because they are derived from changes in sound velocities. However, phonon modes other than those probed by sound velocities (*e.g.*, high-frequency phonon modes) may soften at different rates with temperature. To capture these contributions to the phonon entropy, we have introduced the exponent  $\eta$  in Equation 14 as a corrective factor. This exponent allows for variance in softening between high and low-frequency phonons, while maintaining  $\beta_p(T_0) = 1$  at  $T_0$ . The choice of  $\eta$  reflects the frequency distribution of phonon softening, and is found (below) to be correlated with the Poisson's ratio.

### Accounting for Electronic Entropy

Since we ultimately seek to model the total heat capacity, we must quantify the total entropy. In non-magnetic materials, this requires considering the electronic entropy. For this work, we assume the electronic contribution to the specific heat follows the Sommerfeld approximation, expressed as  $C_{v,\text{el}}(T) = \gamma_{\text{el}}T$  with  $\gamma_{\text{el}}$  as a constant, then the complete specific heat within the quasiharmonic approximation is represented by:

$$C_p^{\text{QHA}}(T) = C_{p,\text{ph}}^{\text{QHA}}(T) + \gamma(T)\gamma_{\text{el}}T. \quad (15)$$

The factor  $\gamma(T)$  in Equation (15), defined as

$$\gamma(T) = \frac{C_p(T)}{C_v(T)} = \frac{B_S(T)}{B_T(T)}, \quad (16)$$

serves as a small correction, reflecting the fact that the Sommerfeld coefficient is traditionally defined at constant volume rather than at constant pressure.

Following a similar approach to Equation 15, we introduce the Sommerfeld term in our elastic softening approximation:

$$C_p^{\text{ESA}}(T) = C_{p,\text{ph}}^{\text{ESA}}(T) + \gamma(T)\gamma_{\text{el}}T, \quad (17)$$

to account for electronic contributions to specific heat.

## APPLICATION TO ELEMENTAL SOLIDS

### Regular Elemental Solids

Figure 2 compares the calculated values of  $C_p^{\text{QHA}}(T)$  and  $C_p^{\text{ESA}}(T)$  using the quasiharmonic and elastic softening approximations against experimental specific heat data for various non-actinide elemental solids which adopt a range of crystal structures:  $\alpha$ -Be [49, 50], diamond [51–53], Al [54–58], Cu [57–61], In [62–65], W [57, 59, 66–73], Au [74–76], and Pb [77].

For the quasiharmonic approximation, the experimental volume, thermal expansivity, and isothermal bulk

modulus data used to calculate  $C_p^{\text{QHA}}(T)$  via Equation (3) are detailed in Appendix A. The phonon density of states measurement temperatures ( $T_0$ ), along with the volume and isothermal bulk moduli at these temperatures, are listed in Table I. The Sommerfeld coefficients [78] employed in Equation 15 are also provided in Table I.

Figure 2 demonstrates that the quasiharmonic approximation aligns well with the experimental behavior of  $C_p(T)$  for elements like Al, Cu, and In. However, for most solids, particularly at higher temperatures, this approximation fails to match the experimental curves. For instance, in cases like  $\alpha$ -Be, diamond, and W, the quasiharmonic approximation significantly underestimates  $C_p(T)$ , whereas, for Au and Pb, it overestimates  $C_p(T)$ .

Conversely, our elastic softening approximation has successfully replicated the observed behavior of  $C_p(T)$  for all elemental solids in Fig. 2 by finding specific values of  $\eta$  (listed in Table I). The calculated  $\beta_p(T)$  curves, derived from Equation 14, are displayed in Fig. 4. These values of  $\eta$ , along with their margins of error determined via a least squares analysis described in Appendix B, suggest that the elastic softening approximation provides a more accurate model for specific heat behavior, particularly at high temperatures. It is especially noteworthy that the ESA works well for elements such as W which are known to have large anharmonic contributions [47]. The adiabatic bulk and shear moduli,  $B_S(T)$  and  $G_S(T)$ , respectively, used for each elemental solid, are shown in Fig. 3, with the rationale for their selection detailed in Appendix C.

### Actinide Elemental Solids

An important characteristic distinguishing actinide elemental solids from non-actinides, as observed in Table I, is their notably larger Sommerfeld coefficients [93, 94]. In actinides, if the electronic entropy were to follow the conventional form  $S_{\text{el}} \approx \gamma_{\text{el}}T$ , Fig. 5 suggests that at higher temperatures, the entropy would reach or exceed the maximum values typical for an ideal half-filled electronic band ( $R \ln 4$ ) or for a lattice of twofold degenerate spins ( $R \ln 2$ ), characteristic of a Kondo lattice system [95]. This observation implies that the assumption of a constant  $\gamma_{\text{el}}$  becomes untenable in actinides like  $\alpha$ -U,  $\alpha$ -Pu, and  $\delta$ -Pu at elevated temperatures.

For  $\delta$ -Pu, various studies have suggested contributions to  $C_p(T)$  from sources beyond phonons, such as local moments or narrow electronic bands [11, 26, 96, 97]. These contributions significantly impact the entropy, with their effects prominent below room temperature and diminishing at higher temperatures. Similar observations have been made for  $\alpha$ -Pu [26]. In the case of  $\alpha$ -U, the  $\gamma_{\text{el}}$  value in Table I is linked to a phase with a reconstructed Fermi surface due to charge-density waves below approximately

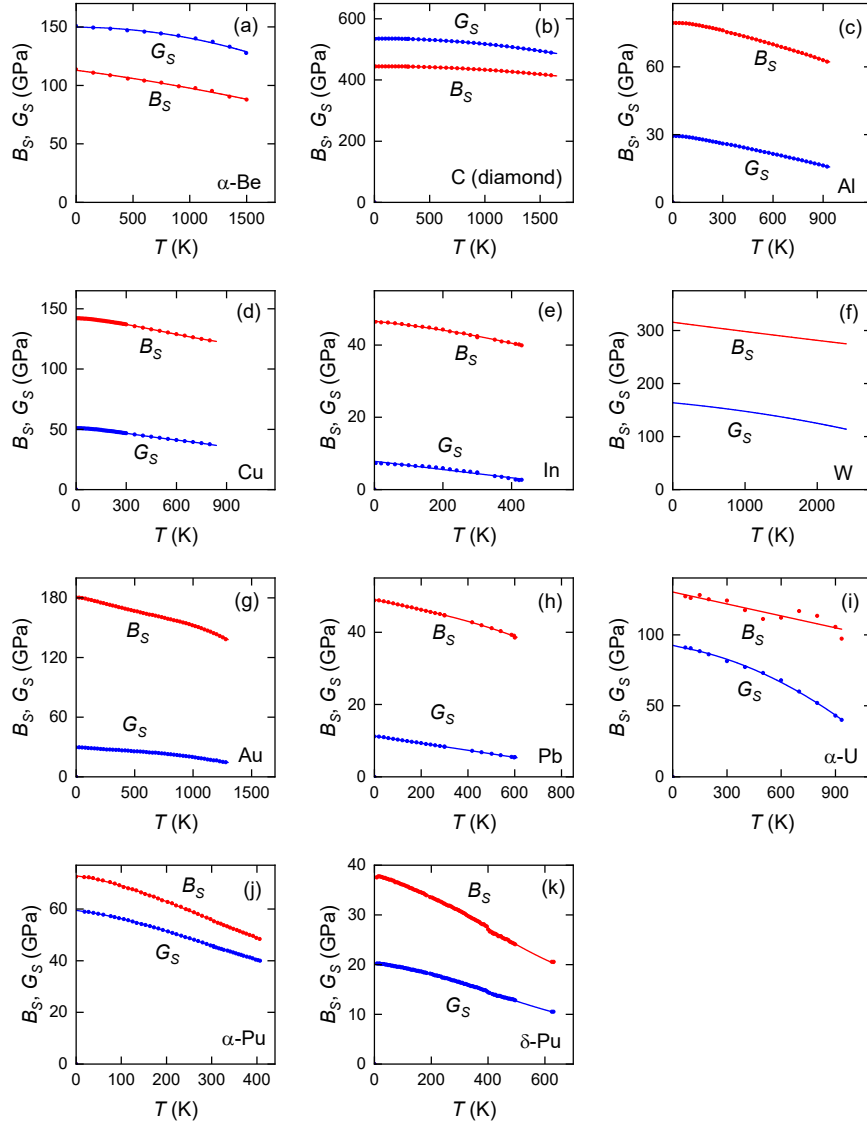


FIG. 3: Adiabatic bulk modulus  $B_S(T)$  and shear modulus  $G_S(T)$  for  $\alpha$ -Be [79] (a), C (diamond) [80, 81] (b), Al[82, 83] (c), Cu [84, 85] (d), In [86, 87] (e), W [88] (f), Au [85, 89] (g), Pb [87, 90] (h),  $\alpha$ -U [91] (i),  $\alpha$ -Pu [16] (j), and  $\delta$ -Pu [16, 92] (k) from various sources, as indicated. For  $\delta$ -Pu, measurements below 500 K pertain to samples where the  $\delta$  phase has been stabilized down to low temperatures by adding 2 atomic percent Ga. Circles represent data points (see Appendix B for details). To bridge gaps between data points and minimize the impact of scatter in the experimental data on thermodynamic derivatives,  $B_S(T)$  and  $G_S(T)$  are approximated with polynomial fits (solid lines).

40 K [93], suggesting a significant residual  $\gamma_{el}$  value in the absence of this order. Despite the nature—magnetic or electronic—of these additional entropy sources in the actinides, the high  $\gamma_{el}$  values suggest an electronic entropy saturation at lower temperatures, thereby excluding a substantial electronic contribution to  $C_p(T)$  at elevated temperatures.

In Fig. 6, we compare  $C_{p,ph}^{ESA}(T)$  and  $C_{p,ph}^{QHA}(T)$  against experimental data for  $\alpha$ -U [98, 99],  $\alpha$ -Pu [26, 28, 45, 94, 100, 101], and  $\delta$ -Pu [28] only at high temperatures (the region shaded in yellow). In pure Pu, the  $\delta$  phase exists only within a temperature range of approximately 580 K to 620 K [13, 14]. We have therefore included data

from Pu samples in which the  $\delta$  phase is stabilized down to lower temperatures by the substitution of 2 or more atomic percent of the Pu atomic sites with Al or Ga [102], as indicated [26, 27, 94, 96, 100]. Our analysis is consistent with a minor electronic contribution at elevated temperatures, which we illustrate by approximating contributions from electronic or magnetic degrees of freedom in actinides with a Schotte-Schotte anomaly [103] (magenta curves in Fig. 6), similar to those discussed in Ref. [26] (see Appendices D and E). The electronic contribution to  $C_p(T)$  in the yellow shaded region at high temperatures from an anomaly at low temperatures is shown to be small.

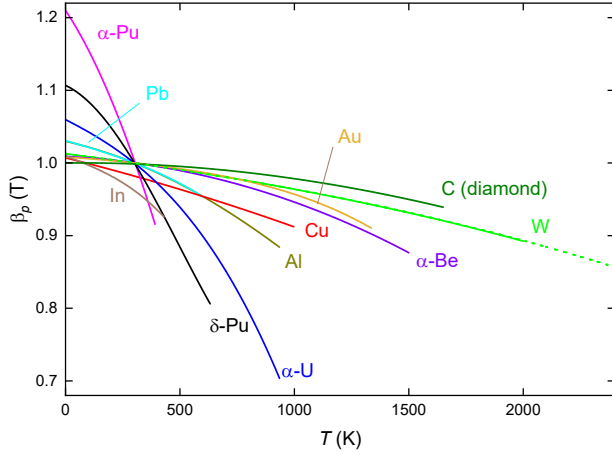


FIG. 4: The softening parameter  $\beta_p(T)$  for each elemental solid determined using Equation 14. Each line corresponds to a different elemental solid, as indicated.

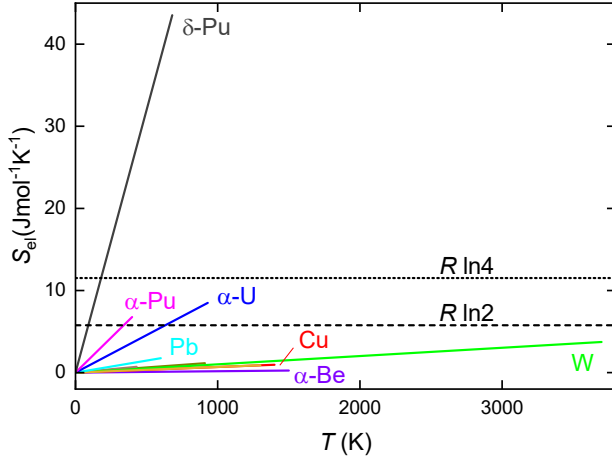


FIG. 5: Estimated Sommerfeld contribution to the entropy  $S_{el}(T)$  under the assumption that the electronic contribution to  $C_p(T)$ , as given by Equations 15 and 17, continues to follow the Sommerfeld form at elevated temperatures.

By utilizing  $\eta$  values consistent with those of regular elemental solids (Table I), the elastic softening approximation accurately reflects the experimentally observed specific heat, unlike the quasiharmonic approximation, which significantly underestimates the phonon contribution at high temperatures and overestimates it at low temperatures. The differences in the performance of these two approximations are further elucidated in Appendix D through a residuals analysis.

### Validation of the Elastic Softening Approximation

Beyond reproducing the temperature dependence of the specific heat in a range of elements solids, there are two key observations that support the accuracy of our elastic softening approximation in understanding anoma-

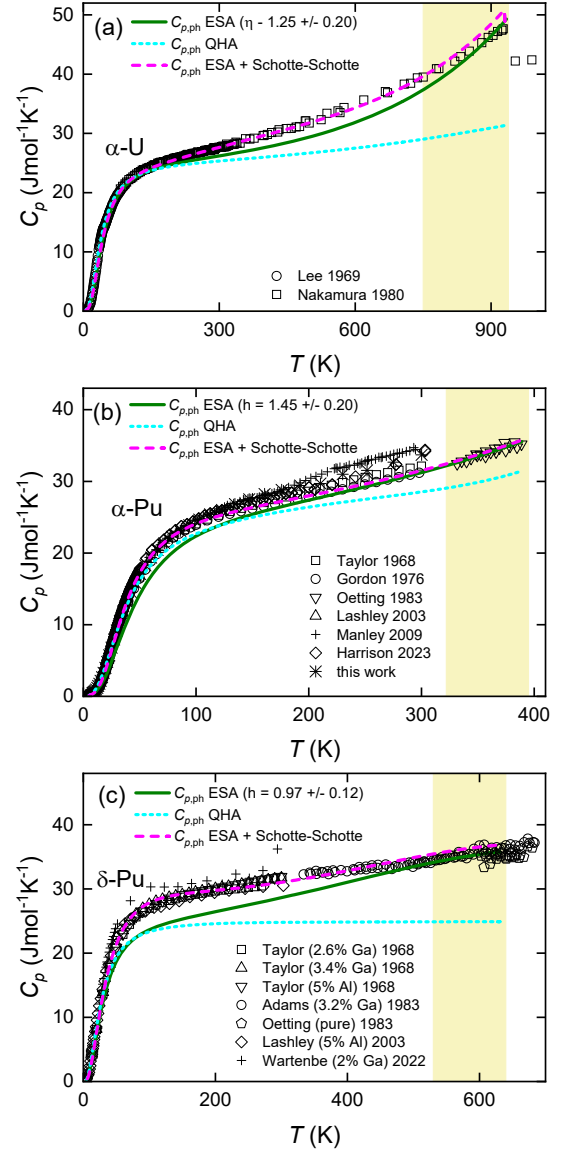


FIG. 6: Specific heat data (represented by symbols) for  $\alpha$ -U (a),  $\alpha$ -Pu (b), and  $\delta$ -Pu (c), sourced from various references [26–28, 45, 94, 96, 98–101], as indicated. The dotted cyan lines represent  $C_{p,ph}^{QHA}(T)$  calculated under the quasiharmonic approximation (QHA) using Equation 3. The solid green lines represent  $C_{p,ph}^{ESA}(T)$  calculated under the elastic softening approximation (ESA) using Equation 7. The dashed magenta curves illustrate  $C_{p,ph}^{ESA}(T)$  combined with a contribution from a Schotte-Schotte anomaly, demonstrating the potential contribution from electronic or magnetic degrees of freedom. The yellow shaded region indicates high temperatures, which are the focus of our analysis (see text).

lous phonon contributions to the specific heat of elemental solids, particularly at elevated temperatures. First, we find consistency between the phonon frequency softening parameter  $\beta_p(T)$  and the experimental temperature-dependent phonon density of states. Figure 7 shows the locations of maxima within the phonon density of states for various materials, obtained from neutron scattering



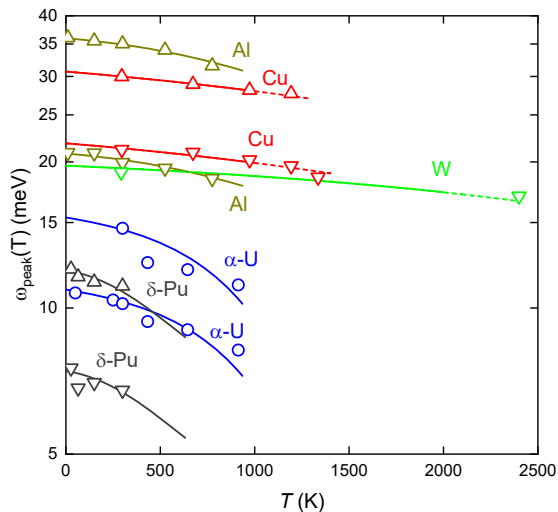


FIG. 7: The measured temperature dependences of prominent features in the phonon density of states (DOS) determined by neutron scattering [7, 17, 20–22] for Al, Cu, W,  $\alpha$ -U, and  $\delta$ -Pu, as indicated by symbols. Lines represent  $\omega_{\text{peak}}(T) = \omega_{\text{peak}}(T_0)\beta_p(T)$ , where  $\omega_{\text{peak}}(T_0)$  is used to rescale  $\beta_p(T)$  from Fig. 4. Dashed lines indicate extrapolations. Upward-pointing triangles denote features in the DOS predominantly associated with longitudinal phonon modes, while downward-pointing triangles indicate features primarily arising from transverse phonon modes. Circles are used to identify features in the phonon DOS that are attributed primarily to optical phonon modes [104].

studies [7, 17, 20–22, 104]. These maxima’s temperature dependences conform well to  $\omega_{\text{peak}}(T) = \omega_{\text{peak}}(T_0)\beta_p(T)$ , where  $\omega_{\text{peak}}(T_0)$  is a constant used to rescale  $\beta_p(T)$  from Fig. 4. For W and Cu, we extrapolate  $\beta_p(T)$  (from the lines in Fig. 4) to compare with frequency shifts from high-temperature experimental data [21]. In the case of Cu, the frequency shifts pertain to the maxima of the longitudinal and transverse phonon dispersions [20], which contribute maximally to the peaks in the phonon density of states. The ability of the phonon softening parameter  $\beta_p(T)$  to successfully reproduce the temperature dependence of high-frequency portions of the phonon density of states lends credence to our approach of scaling low-frequency phonon softening, provided by elastic moduli measurements, to model the entire temperature-dependent phonon density of states.

Second, the values of  $\eta$  for the elemental solids investigated within this work are not random, but correlated with the nature of the bonding in the elemental solids. This is evidenced by the direct correlation between  $\eta$  and Poisson’s ratio shown in Fig. 8. Poisson’s ratio describes the transverse strain arising in response to a longitudinal strain [24]. In general this will be an anisotropic quantity, but for an isotropic crystal it is related to the bulk and shear elastic moduli through

$$\nu = \frac{3B_S - 2G_S}{6B_S + 2G_S}. \quad (18)$$

Poisson’s ratio is also temperature dependent, reflecting the temperature dependence of the underlying elasticity.

As a ratio of elastic moduli,  $\nu$  is known to provide a good indication of the type of interatomic bonding present within a solid [23, 25]. For isotropic solids, three cases are typically considered [105–107]: (1)  $\nu = 0.25$  corresponding to interatomic bonding mediated through a central force potential; (2)  $\nu > 0.25$  indicating the presence of more metallic bonding character; (3)  $\nu < 0.25$  pointing towards more covalent bonding character. Since it reflects bonding character, Poisson’s ratio is also often used as a proxy for intrinsic ductility ( $\nu > 0.25$ ) and brittleness ( $\nu < 0.25$ ) [108–110].

The Poisson’s ratio values shown in Fig. 8 were evaluated using Equation 18 in the limit  $T \rightarrow 0$ . The linear trend in Fig. 8 reveals a physical relationship linking anomalous phonon contributions to  $C_p(T)$  with the bonding character of solids. Notably, actinide solids also align with this trend, confirming our finding that phonon degrees of freedom largely account for their specific heat at elevated temperatures. The dotted line in Fig. 8 indicates an approximately linear relationship:

$$\eta(\nu) = b(\nu_0 - \nu), \quad (19)$$

with  $\nu_0 = 0.485 \pm 0.034$  and  $b = 4.40 \pm 0.30$ . The larger error bars for diamond reflect limited high-temperature data. This relationship between  $\nu$  and  $\eta$  suggests that metallic bonding character reduces the contribution of elastic moduli changes to the phonon softening parameter  $\beta_p$  such that only the volumetric term remains in Equation 14 when  $\nu \approx 0.5$ . Alternatively, the elastic moduli changes provide larger contributions to  $\beta_p$  with increased covalent bonding character.

### Ascertaining the Anharmonic Contribution

In Fig. 9, we present a comprehensive comparison of phonon contributions to the specific heat beyond the harmonic approximation for each of the elemental solids, including the actinides. Figure 9(a) illustrates the quasiharmonic contribution, denoted as  $\Delta C^{\text{QHA}}(T) = C_{p,\text{ph}}^{\text{QHA}}(T) - C_{v,\text{ph}}^{\text{HA}}(T) = V(T)\alpha_v^2(T)B_T(T)T$ . Figure 9(b) displays the additional anomalous softening contribution,  $\Delta C^{\text{AN}}(T) = C_{p,\text{ph}}^{\text{ESA}}(T) - C_{p,\text{ph}}^{\text{QHA}}(T)$ , which is captured by our elastic softening approximation, but not by the quasiharmonic approximation.

To the extent that  $C_{p,\text{ph}}^{\text{QHA}}$  accurately captures the quasiharmonic contribution to the specific heat, it is reasonable to propose that  $\Delta C_p^{\text{AN}}(T)$  approximates the specific heat contribution due to intrinsic anharmonicity.

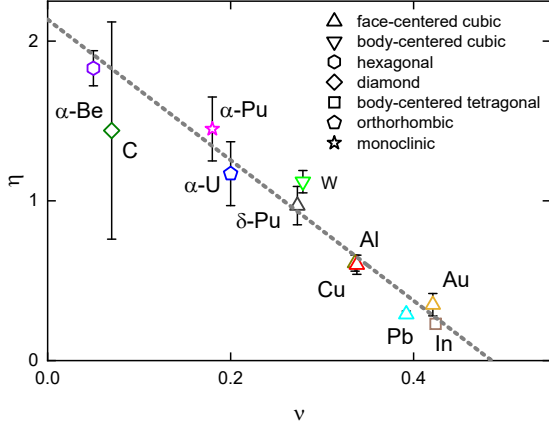


FIG. 8: The differential softening parameter  $\eta$ , along with its error bars, is plotted against Poisson's ratio  $\nu$  for each elemental solid. Different symbol shapes in the plot correspond to various crystal structures, as indicated.

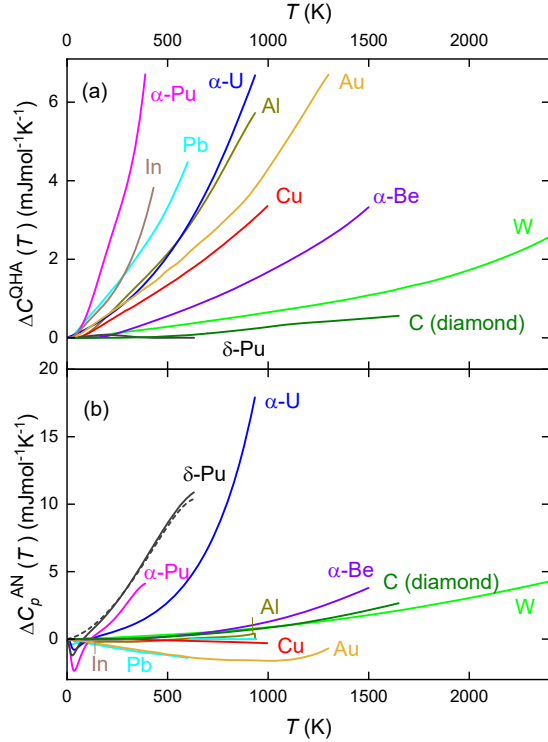


FIG. 9: A comparison of  $\Delta C_p^{\text{QHA}}(T)$  (a) and  $\Delta C_p^{\text{AN}}(T)$  (b), as defined in the text. The dashed line in (b) represents  $\Delta C_p^{\text{AN}}(T)$  for  $\delta$ -Pu, estimated using  $a(T)$  as given by Equation 21.

This association is particularly robust in the case of  $\delta$ -Pu, where the volume change with temperature is minimal. This interpretation is supported by a standard definition of intrinsic anharmonicity [9, 111]:

$$a(T) = \left. \frac{\partial \ln \omega(T)}{\partial T} \right|_v. \quad (20)$$

Given the near-constant volume of  $\delta$ -Pu, we can approximate that  $\partial \omega(T)/\partial T|_v \approx \partial \omega(T)/\partial T|_p$ . This allows for

the substitution  $\beta_p(T) \propto \omega(T)$ , as indicated in Equation 4, leading to:

$$a(T) \approx \frac{\partial \ln \beta_p(T)}{\partial T}. \quad (21)$$

Using the approximation  $\Delta C_p^{\text{AN}} = 3a(T)RT$  for intrinsic anharmonic phonon contributions to the specific heat [18, 111], we arrive at the dashed line in Fig. 9(b). This line is consistent with the form obtained using  $\Delta C_p^{\text{AN}}(T) = C_{p, \text{ph}}^{\text{ESA}}(T) - C_{p, \text{ph}}^{\text{QHA}}(T)$ , thus validating our approach for quantifying the anharmonic contributions in  $\delta$ -Pu.

## DISCUSSION

A significant limitation of the quasiharmonic approximation is, despite its widespread success in certain materials [5], its neglect of intrinsic anharmonicity. Intrinsic anharmonicity is often considered to be important under extreme conditions of high temperature and pressure [8], but it can also be significant in scenarios where the thermal expansivity at constant pressure is small or negative [9]. In the particular case of  $\delta$ -Pu, this oversight fails to capture the primary mechanism of phonon softening with temperature [17]. Our proposed elastic softening approximation, based on an approach developed by Wallace [18], effectively treats such scenarios.

A pivotal aspect of our approach is capturing the varying rates of softening of the phonon density of states at different frequencies, relative to the behavior observed in elastic moduli measurements which only directly probe the phonon density of states near  $\omega \approx 0$ . To account for the thermodynamic effect of this differential softening at high temperatures, we have introduced the parameter  $\eta$ . This parameter is not arbitrary; it exhibits a pronounced correlation with Poisson's ratio (shown in Fig. 8). This finding suggests that  $\eta$  exceeds one in materials with more covalent bonding character and is smaller in materials with more metallic bonding character. Given that Poisson's ratio is a well-established metric across all solids [23–25], we anticipate our elastic softening approximation can be used as a more accurate predictor of the phonon contribution to specific heat, inclusive of anharmonic effects, than the quasiharmonic approximation. Importantly, the correlation of  $\eta$  with  $\nu$  enables its use in predicting the specific heat profile over a broad temperature range without needing adjustable parameters.

The robustness of our method is further endorsed by the strong correlation between the overall phonon softening,  $\beta_p(T)$ , and the softening of high-energy spectral features in the phonon density of states, as inferred from neutron scattering measurements (shown in Fig. 7). The parallel trends in the softening of both longitudinal and transverse modes at high frequencies justify our method's

assumptions and the application of the weighted average approximation in Equation 14.

A critical aspect of our study is the use of the actual phonon density of states (as presented in Fig. 1) and the measured temperature-dependent elastic moduli (Fig. 3), rather than approximations based on the Debye or Einstein models [6]. While the Debye or Einstein model-based approaches can model the temperature dependence of  $C_p(T)$  by introducing multiple adjustable parameters, they might conceal the true extent of phonon softening and the novel physics underlying them (as revealed in Figs. 7, 8, and 9).

The findings presented in Fig. 9 indicate that an intrinsic anharmonic phonon contribution to the specific heat is not only significant in  $\delta$ -Pu, but also prominently present in all three actinide solids we studied. It is crucial to emphasize that in these materials, electronic degrees of freedom primarily contribute to the specific heat at low temperatures (see Appendices D and E). This deviates from typical elemental solids where the Sommerfeld approximation usually suffices [6].

For  $\delta$ -Pu, its minimal thermal expansivity enables a quantifiable analysis of its intrinsic anharmonic contribution to the specific heat, as demonstrated in Fig. 9, in line with previous estimates based on theoretical modeling [11]. For  $\alpha$ -Pu, our findings align with earlier reports suggesting anharmonicity [11, 112]. However, in the case of  $\alpha$ -U, despite its significant thermal expansivity, the phonons have been suggested to remain harmonic [22]. Future work will be needed to understand these differences in  $\alpha$ -U.

One factor believed to play a significant role in the actinides is the interaction between phonons and electronic degrees of freedom. For instance, the negative thermal expansivity observed in  $\delta$ -Pu is thought to be the result of electronic or magnetic mechanisms [15, 113–115], which might also contribute to phonon softening [114]. In  $\alpha$ -U, the notable softening of phonons with temperature increase is suggested to stem from strong electron-phonon coupling [116]. Importantly, despite the potential influence of electronic degrees of freedom, the correlation between the parameter  $\eta$  and Poisson's ratio continues to hold (as shown in Fig. 9).

Our comparative analysis of temperature-induced changes in the elastic moduli of  $\delta$ -Pu and other face-centered cubic solids reveals a unique trait in  $\delta$ -Pu. In contrast to the typical behavior of face-centered cubic materials (see Fig. 3), where a more rapid reduction in shear modulus relative to bulk modulus is seen,  $\delta$ -Pu maintains an almost constant shear-to-bulk modulus ratio with increasing temperature [16]. This characteristic, differing from expectations for a material with a crystal structure similar to highly ductile elements, implies a greater degree of covalency in  $\delta$ -Pu. This observation is in line with the larger  $\eta$  value found for  $\delta$ -Pu compared to other face-centered cubic elemental solids. The resis-

tance to shear deformation in  $\delta$ -Pu, reminiscent of materials like  $\alpha$ -Be and diamond known for their rigid covalent bonding, suggests a mechanism potentially related to the coupling of  $5f$ -electrons to the crystal lattice symmetry. This hypothesis gains further support from the similar temperature dependence of shear and bulk moduli in  $\alpha$ -Pu, as shown in Fig. 3, which exhibits greater brittleness than  $\delta$ -Pu.

## APPENDIX A: PARAMETERS USED IN THE QUASIHARMONIC APPROXIMATION

In our study, Figures 10(a) and (b) respectively illustrate the normalized volume  $V(T)/V(T_0)$  and thermal expansivity  $\alpha_v(T)$ , which are key parameters in calculating  $C_{p,\text{ph}}^{\text{QHA}}(T)$  using the quasiharmonic approximation [26, 35, 50, 71, 117–124]. Additionally, Fig. 11 displays the temperature-dependent ratio of bulk modulus,  $B_T(T)/B_T(T_0)$ . For Al, Cu, W, and Pb, we have relied on experimental  $B_T(T)$  values [35, 119, 120, 122] that align with equation of state modeling.

For materials such as  $\alpha$ -Be, diamond, In, Au,  $\alpha$ -U,  $\alpha$ -Pu, and  $\delta$ -Pu, we calculated  $B_T(T)$  using Equation (22):

$$\gamma(T) = \frac{B_S(T)}{B_T(T)} = 1 + \frac{V(T)\alpha_v^2(T)B_S(T)T}{C_p(T)}. \quad (22)$$

This calculation involves published values of  $B_S(T)$  (shown in Fig.3) and  $C_p(T)$  [28, 50, 98, 99, 101]. The resulting  $\gamma(T)$  values, independent of the specific approximation used (quasiharmonic or elastic softening), are graphically represented in Fig. 12.

## APPENDIX B: LEAST SQUARES ANALYSIS METHOD

For each elemental solid, the value of  $\eta$  was estimated utilizing a least squares analysis method, wherein  $\eta$  is iteratively adjusted until the summation

$$b(\eta) = \sum_i (C_p^{\text{ESA}}(T_i) - C_p(T_i))^2 \quad (23)$$

is minimized. In this equation,  $i$  refers to individual specific heat data points  $C_p(T_i)$  taken at a temperature  $T_i$ . To estimate the error bars for each elemental solid, we assessed the change in  $\eta$  necessary to double  $b$ . For elemental solids with multiple published specific heat datasets, discrepancies between these datasets led to larger uncertainties in determining  $\eta$ .

## APPENDIX C: VALUES OF THE ADIABATIC BULK AND SHEAR MODULI

In  $\alpha$ -U,  $\alpha$ -Pu and  $\delta$ -Pu,  $B_S(T)$  and  $G_S(T)$  were determined from measurements of polycrystalline sam-

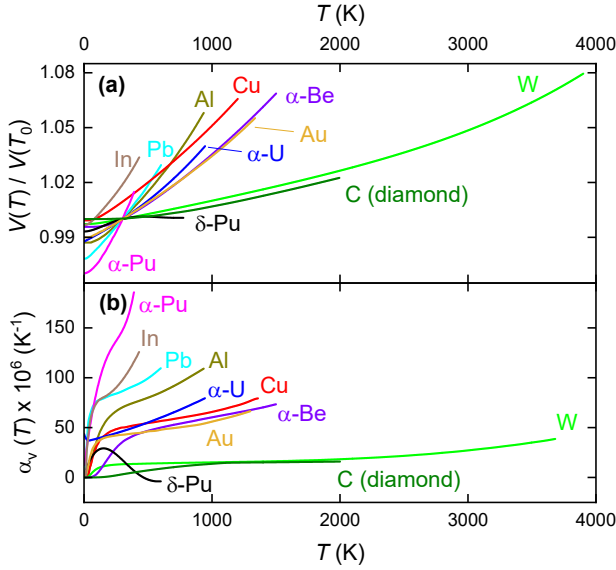


FIG. 10: Renormalized volume  $V(T)/V(T_0)$  (a) and thermal expansivity  $\alpha_v(T)$  (b) of  $\alpha$ -Be [50], C (diamond) [117], Al [118, 119], Cu [71, 120], In [121], W [122], Au [123], Pb [35],  $\alpha$ -U [124],  $\alpha$ -Pu [26] and  $\delta$ -Pu [26] as indicated. Values of  $T_0$  and  $V(T_0)$  are listed in Table I.

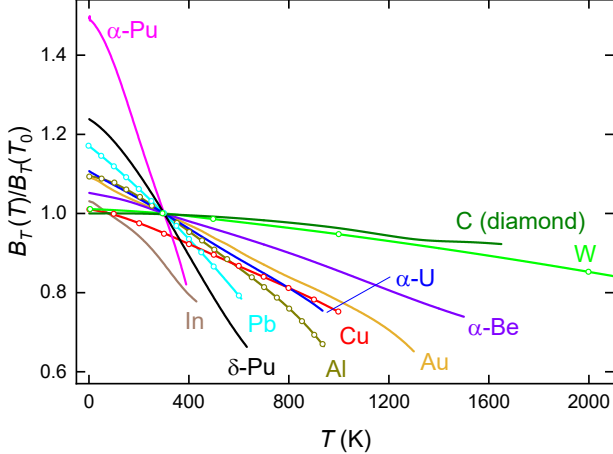


FIG. 11: Renormalized isothermal bulk modulus  $B_T(T)/B_T(T_0)$  of  $\alpha$ -Be, Al [119], Cu [120], W [122], Pb [35],  $\alpha$ -U,  $\alpha$ -Pu and  $\delta$ -Pu as indicated. Values of  $T_0$  and  $B_T(T_0)$  are listed in Table I.

ples [16, 91]. In order to facilitate a direct comparison between different elemental solids with different crystalline structures, we have used  $B_S(T)$  and  $G_S(T)$  throughout. In the cases of diamond, Al, Cu, In, W, Au and Pb,  $B_S(T)$  and  $G_S(T)$  were estimated from elastic moduli measurements on single crystals. This was done by taking the geometric means of  $B_S(T)$  and  $G_S(T)$  estimated using the Voigt [125] and Reuss [126] methods, as suggested by Hill [127]. Polynomials were used to fit  $B_S(T)$  and  $G_S(T)$ . The parameters are listed in Table II.

In the case of Al, Cu, In, W and Pb, the elastic moduli were measured using an ultrasonic pulse-echo tech-

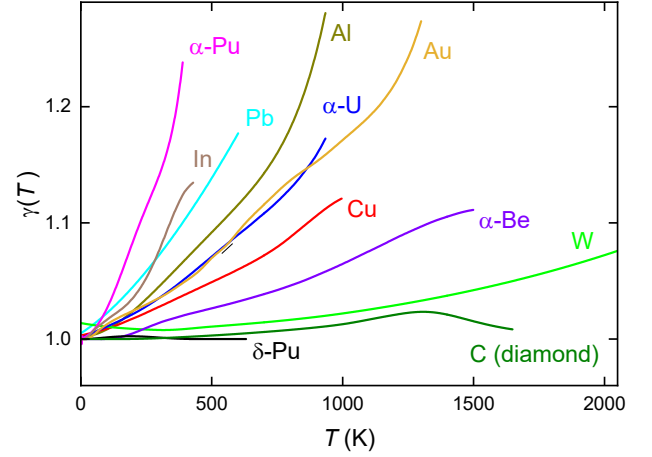


FIG. 12: Values of  $\gamma(T)$  obtained using Equation (16).

nique [82–87, 89, 90]. In the case of C (diamond), the elastic moduli below room temperature were measured using resonant ultrasound spectroscopy [81], whereas the elastic moduli above room temperature were estimated using Brillouin scattering [80]. In  $\alpha$ -Be,  $B_S(T)$  and  $G_S(T)$  were estimated by means of high rate straining [79]. In  $\alpha$ -Pu and  $\delta$ -Pu,  $B_S(T)$  and  $G_S(T)$  were measured using resonant ultrasound spectroscopy [16]. In  $\alpha$ -U, meanwhile,  $B_S(T)$  and  $G_S(T)$  were measured using a thin rod resonance method [91].

#### APPENDIX D: SPECIFIC HEAT RESIDUALS FOR THE ACTINIDE ELEMENTAL SOLIDS

Figure 13 illustrates that only through our elastic softening approximation method does the difference between the experimental  $C_p(T)$  and the computed  $C_{p,\text{ph}}(T)$  yield a residual specific heat versus temperature, which aligns closely with a physically plausible non phonon contribution. In contrast, the quasiharmonic approximation tends to overestimate the phonon contribution to  $C_p(T)$  at lower temperatures, leading to negative residuals for  $(C_{p,\text{ph}}^{\text{QHA}}(T) - C_{p,\text{ph}}(T))/T$  in Pu. The observed peaks in  $(C_{p,\text{ph}}^{\text{ESA}}(T) - C_{p,\text{ph}}(T))/T$  for  $\alpha$ -Pu and  $\delta$ -Pu could indicate several possibilities, such as a Schottky anomaly related to an energy gap or magnetic energy levels [128], a Schotte-Schotte anomaly [103] from a resonance feature in the electronic density of states [26], or the emergence of Kondo singlets [97].

In the case of  $\alpha$ -U, considering  $B_S(T)$  and  $G_S(T)$  values only above 50 K, to circumvent discontinuities associated with charge-density wave phases, results in negative residuals at lower temperatures, even when employing our elastic softening approximation. Despite these limitations below approximately 50 K, the phase transition anomaly associated with the charge-density waves becomes distinctly evident in  $(C_{p,\text{ph}}^{\text{ESA}}(T) - C_{p,\text{ph}}(T))/T$ ,

element	$B_0$	$B_1$	$B_2$	$B_3$	$G_0$	$G_1$	$G_2$	$G_3$
$\alpha$ -Be	112.962	-0.0128315	$-2.45854 \times 10^{-6}$	0	149.726	$-6.05829 \times 10^{-5}$	$-9.28125 \times 10^{-6}$	0
diamond	444.197	0.00274012	$-1.4784 \times 10^{-5}$	$1.06515 \times 10^{-9}$	535.059	0.00266921	$-2.14913 \times 10^{-5}$	$1.24698 \times 10^{-9}$
Al	79.7224	-0.00663411	$-2.22926 \times 10^{-5}$	$1.00555 \times 10^{-8}$	29.6112	-0.00872952	$-1.0797 \times 10^{-5}$	$4.58994 \times 10^{-9}$
Cu	142.235	-0.00787221	$-3.93485 \times 10^{-5}$	$2.56058 \times 10^{-8}$	51.1213	-0.00831371	$-2.55544 \times 10^{-5}$	$1.88028 \times 10^{-8}$
In	46.5552	-0.00947208	$-1.42592 \times 10^{-5}$	0	7.83453	-0.0114104	0	0
W	315.627	-0.0177789	$3.43707 \times 10^{-7}$	0	163.69	-0.012698	$-3.33073 \times 10^{-6}$	0
Au	181.641	-0.0358176	$2.04844 \times 10^{-5}$	$-1.44161 \times 10^{-8}$	29.2705	-0.0038301	$-5.81716 \times 10^{-6}$	0
Pb	48.9957	-0.0135392	$4.78957 \times 10^{-7}$	$-1.02712 \times 10^{-8}$	11.2625	-0.00979439	0	0
$\alpha$ -U	130.111	-0.0279822	0	0	92.1994	-0.0200572	$-3.79219 \times 10^{-5}$	0
$\alpha$ -Pu	72.8813	-0.0231165	-0.000174498	$2.05688 \times 10^{-7}$	59.4488	-0.0200056	-0.000130367	$1.53013 \times 10^{-7}$
$\delta$ -Pu	37.8123	-0.0114931	$-5.62579 \times 10^{-5}$	$4.81719 \times 10^{-8}$	20.2357	-0.00511441	$-3.35896 \times 10^{-5}$	$2.70191 \times 10^{-8}$

TABLE II: Polynomial fit parameters for  $B_S(T)$  and  $G_S(T)$ , where  $B_S(T) = B_0 + B_1T + B_2T^2 + B_3T^3$  and  $G_S(T) = G_0 + G_1T + G_2T^2 + G_3T^3$ . The units are in GPa.

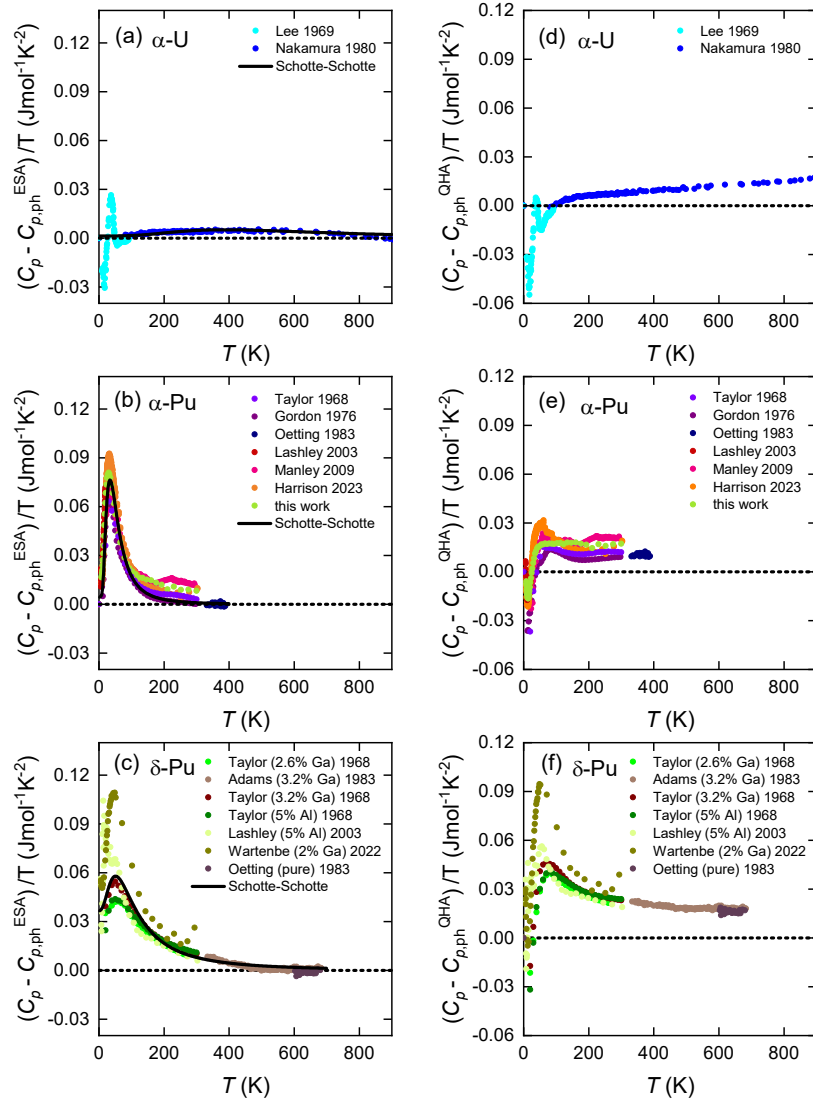


FIG. 13: The residual specific heat divided by temperature after having subtracted  $C_{p,\text{ph}}^{\text{ESA}}(T)$  in  $\alpha$ -U (a),  $\alpha$ -Pu (b) and  $\delta$ -Pu (c), and after having subtracted  $C_{p,\text{ph}}^{\text{QHA}}(T)$  in  $\alpha$ -U (d),  $\alpha$ -Pu (e) and  $\delta$ -Pu (f). Black solid lines in (a), (b) and (c) depict a Schotte-Schotte anomaly (discussed in Appendix E).

as shown in Fig. 13(a).

### APPENDIX E: CONTRIBUTION FROM ELECTRONIC OR MAGNETIC DEGREES OF FREEDOM

For illustrative purposes, we utilize the Schotte-Schotte anomaly model [103] to approximate possible contributions from magnetic or electronic degrees of freedom in actinide solids. This model may be relevant when considering excitations between different magnetic energy states or sharp features in the electronic density of states of an insulator or metal, offset relative to the chemical potential. If the energy levels are infinitely sharp, the result is a Schottky anomaly [129]. In cases where these levels are broadened, creating a Lorentzian-shaped feature in the electronic density of states, the resultant specific heat feature aligns with the functional form of a Schotte-Schotte anomaly [103]. Originally proposed for  $f$ -electron compounds in strong magnetic fields, this model accounts for specific heat contributions in scenarios where a Kondo resonance undergoes Zeeman splitting.

The specific heat contribution of such an anomaly is described by

$$C_{\text{el}}(T) \approx \frac{R}{k_{\text{B}}} \frac{\partial}{\partial T} \left[ \int_{-\infty}^{\infty} \varepsilon D_{\text{el}}(\varepsilon) f(\varepsilon/T) d\varepsilon \right], \quad (24)$$

where

$$D_{\text{el}}(\varepsilon) = \frac{\eta\Gamma}{\pi((\varepsilon - \mu \pm \Delta)^2 + \Gamma^2)}$$

takes the form of a Lorentzian, and  $\varepsilon$  is the energy. The spectral weight  $w$  of the anomaly, and the parameters  $\Delta$  and  $\Gamma$ , representing the energy gap and the width of the Lorentzian, respectively, define the anomaly's line shape. Specific heat curves resembling a Schotte-Schotte anomaly are common in valence fluctuating systems, often characterized by prominent, lifetime-broadened features in the electronic density of states [130, 131].

In  $\alpha$ -Pu, as shown in Fig. 13(b), the consistency among different measurements allows us to approximate the residual with a Schotte-Schotte anomaly, characterized by parameters  $\Delta = 9.7$  meV,  $\Gamma = 0.6$  meV, and  $w = 0.46$ , similar to findings in Ref. [26]. For  $\delta$ -Pu, variations in the magnitude of the residuals, potentially influenced by Ga or Al concentration, are represented by a broader Schotte-Schotte anomaly, averaging  $\Delta = 17.4$  meV,  $\Gamma = 10.2$  meV, and  $w = 0.94$ . This may also reflect the possibility of a composition-dependent Schottky contribution at higher energies, as suggested in studies related to the invar effect [15, 97]. In the case of  $\alpha$ -U at temperatures above 100 K, a broader anomaly with  $\Delta = 120$  meV,  $\Gamma = 30$  meV, and  $w = 0.6$  is required to approximate the residual. However, this model becomes less representative at lower temperatures, particu-

larly below 40 K, due to the charge-density wave phases in this system.

### APPENDIX F: PREPARATION OF $\alpha$ -PU MATERIAL USED FOR MEASUREMENTS IN THIS WORK

A chunk of  $\alpha$ -Pu was arc-melted in a multi-stage pumped/purged chamber employing a Zr-gettered argon atmosphere. The melting was performed to remove surface oxide present, to allow the  $^4\text{He}$  built up from radioactive decay to be released, and to remove defects formed from self-irradiation damage. Upon completion of arc-melting, the resulting clean button was wrapped into Ta-foil and then sealed within an evacuated fused silica tube. The resulting ampoule was then loaded into a box furnace, which was then ramped to 460 °C, and held there for one month. After one month, the ampoule was furnace cooled to retrieve the button.

### APPENDIX G: $\alpha$ -PU SPECIFIC HEAT MEASUREMENTS PERFORMED IN THIS WORK

Specific heat data using the fresh piece  $\alpha$ -Pu button was collected using a 14-Tesla Quantum Design DynaCool Physical Property Measurement System (PPMS). The semi-adiabatic pulse technique was employed. Contributions of Apiezon N-grease used to mount the sample to the sapphire stage of the Quantum Design specific heat option were subtracted using a separate measurement of the addenda.

### DATA AVAILABILITY

The data that support the findings of this study are available upon reasonable request.

- 
- [1] M.A. Blanco, E. Francisco, V. Luaña, GIBBS: isothermal-isobaric thermodynamics of solids from energy curves using a quasi-harmonic Debye model. *Computer Physics Communications*, **158**, 57-72 (2004).
  - [2] I. V. Lomonosov, Multi-phase equation of state for aluminum. *Laser and Particle Beams* **25**, 567-584 (2007).
  - [3] T. Sjostrom, S. Crockett and S. Rudin, Multiphase aluminum equations of state via density functional theory. *Phys. Rev. B* **94**, 144101 (2016).
  - [4] J. D. McHardy, An introduction to the theory and use of SESAME equations of state, <https://doi.org/10.2172/1487368> (2018).
  - [5] B. Fultz, Vibrational thermodynamics of materials. *Progress in Materials Science* **55**, 247-352 (2010).

- [6] N. W. Ashcroft, N. D. Mermin, *Solid state physics* (Saunders College Publishing, Orlando 1976).
- [7] M. Kresch, M. Lucas, O. Delaire, J. Y. Y. Lin, B. Fultz, Phonons in aluminum at high temperatures studied by inelastic neutron scattering. *Phys. Rev. B* **77**, 024301 (2008).
- [8] M. H. G. Jacobs, B. H. W. S. de Jong, Quantum-thermodynamic treatment of intrinsic anharmonicity; Wallace's theorem revisited. *Phys. Chem. Minerals* **32**, 614-626 (2005).
- [9] M. T. Dove, H. Wang, Negative thermal expansion and associated anomalous physical properties: review of the lattice dynamics theoretical foundation. *Rep. Prog. Phys.* **79**, 066503 (2016).
- [10] D. C. Wallace, Electronic and phonon properties of six crystalline phases of Pu metal. *Phys. Rev. B* **58**, 15433-15439 (1998).
- [11] A. C. Lawson, Thermodynamics of the bulk modulus of delta phase plutonium alloys. *Philosophical Magazine* **99**, 0370-0387 (2019).
- [12] F. Bottin, R. Béjaud, B. Amadon, L. Baguet, M. Torrent, A. Castellano, and J. Bouchet, Huge anharmonic effects in delta plutonium. *Phys. Rev. B* **109**, L060304 (2024).
- [13] E. R. Jette, Some physical properties of plutonium metal. *J. Chem. Phys.* **23** 365-368 (1954).
- [14] F. W. Schonfeld, and R. E. Tate. *The thermal expansion behavior of unalloyed plutonium*, Report LA-13034-MS, Los Alamos National Laboratory (1996).
- [15] A. C. Lawson, J. A. Roberts, B. Martinez, M. Ramos, G. Kotliar, F. W. Trouw, M. R. Fitzsimmons, M. P. Hehlen, J. C. Lashley, H. Ledbetter, R. J. McQueeney and A. Migliori, Invar model for  $\delta$ -phase Pu: thermal expansion, elastic and magnetic properties. *Phil. Mag.* **86**, 2713-2733 (2006).
- [16] Y. Suzuki, V. R. Fanelli, J. B. Betts, F. J. Freibert, C. H. Mielke, J. N. Mitchell, M. Ramos, T. A. Saleh, A. Migliori, Temperature dependence of elastic moduli of polycrystalline  $\beta_p$  plutonium. *Phys. Rev. B* **84**, 064105 (2011).
- [17] R. J. McQueeney, A. C. Lawson, A. Migliori, T.M. Kelley, B. Fultz, M. Ramos, B. Martinez, J. C. Lashley, S. Vogel, Unusual phonon softening in  $\delta$ -phase plutonium. *Phys. Rev. Lett.* **92**, 146401 (2004).
- [18] D. C. Wallace, *Thermodynamics of Crystals* (Wiley, New York 1972).
- [19] M. S. Bryan, J. W. L. Pang, B. C. Larson, A. Chernatynskiy, D. L. Abernathy, K. Gofryk, and M. E. Manley, Impact of anharmonicity on the vibrational entropy and specific heat of  $\text{UO}_2$ . *Phys. Rev. Materials* **3**, 065405 (2019).
- [20] A. Larose, B. N. Brockhouse, Lattice vibrations in copper at elevated temperatures studied by neutron scattering. *Can. J. Phys.* **54**, 1990-2009 (1976).
- [21] V. A. Semenov, O. A. Dubovsky, A. V. Orlov, D. V. Savostin, V. V. Sudarev, Spectrum of vibrational frequencies of crystalline tungsten at temperatures of 293 and 2400 K. *Physics of the Solid State* **56**, 29-33 (2014).
- [22] M. E. Manley, B. Fultz, R. J. McQueeney, C. M. Brown, W. L. Hults, J. L. Smith, D. J. Thoma, R. Osborn, J. L. Robertson, Large Harmonic Softening of the Phonon Density of States of Uranium. *Phys. Rev. Lett.* **86**, 3076-3079 (2001).
- [23] W. Köster and H. Franz, Poisson's Ratio for Metals and Alloys. *Metall. Rev.* **6**, 1-56 (1961).
- [24] G. N. Greaves, A. L. Greer, R. S. Lakes, and T. Rouxel, Poisson's ratio and modern materials. *Nature Mat.* **10** 823-837 (2011).
- [25] H. Ledbetter and A. Migliori, Elastic-constant systematics in f.c.c. metals, including lanthanides-actinides. *phys. stat. sol. (b)* **245**, 44-49 (2008).
- [26] N. Harrison, G. Chappell, P. H. Tobash, Indications of flat bands driving the  $\delta$  to  $\alpha$  volume collapse of plutonium, *Proc. Natl. Acad. USA* (in press 2023).
- [27] R. O. Adams, F. L. Oetting, The chemical thermodynamics of nuclear materials: IX. The high temperature heat capacity of plutonium-3.2 at. % gallium alloy.. *Journal of Nuclear Materials* **118**, 269-274 (1983).
- [28] F. L. Oetting, R. O. Adams, The chemical thermodynamics of nuclear materials VIII. The high-temperature heat capacity of unalloyed plutonium metal. *J. Chem. Thermodynamics* **15**, 537-554 (1983).
- [29] X. Dai, S. Y. Savrasov, G. Kotliar, A. Migliori, Ledbetter, H., E. Abhahams, Calculated phonon spectra of plutonium at high temperatures. *Science* **300**, 953-955 (2003).
- [30] G. Robert, A. Pasturel, B. Siberchicot, Calculated thermodynamic properties of plutonium metal. *J. Phys. Cond. Matt.* **15**, 8377-8387 (2003).
- [31] A. Migliori, H. Ledbetter, A. C. Lawson, A. P. Ramirez, D. A. Miller, J. B. Betts, M. Ramos, J. C. Lashley, Unexpected elastic softening in  $\delta$ -plutonium. *Phys. Rev. B* **73**, 052101 (2006).
- [32] E. R. Cohen, *The Physics Quick Reference Guide* (American, Institute for Physics Press, Woodbury 1996).
- [33] W. B. Holzapfel, M. Hartwig, W. Sievers, Equations of State for Cu, Ag, and Au for Wide Ranges in Temperature and Pressure up to 500 GPa and Above. *J. Phys. Chem. Ref. Data* **30**, 515-529 (2001).
- [34] S. L. Shang, Y. Wang, D. Kim, Z.-K. Liu, First-principles thermodynamics from phonon and Debye model: Application to Ni and  $\text{Ni}_3\text{Al}$ . *Computational Materials Science* **47**, 1040-1048 (2010).
- [35] N. V. Kozyrev, V. V. Gordeev, Thermodynamic characterization and equation of state for solid and liquid lead. *Metals* **12**, 16 (2022).
- [36] R. E. Schmunk, Extension of the dispersion-relation measurements of beryllium. *Phys. Rev.* **149**, 450-456 (1966).
- [37] J. Wormald, A. I. Hawari, Generation of phonon density of states and thermal scattering law using ab initio molecular dynamics. *Progress in Nuclear Energy* **101**, 461-467 (2017).
- [38] A. Bosak, M. Krisch, Phonon density of states probed by inelastic x-ray scattering. *Phys. Rev. B* **72**, 224305 (2005).
- [39] C. B. Walker, X-ray study of lattice vibrations in aluminum. *Phys. Rev.* **103**, 547-557 (1956).
- [40] G. Nilsson and S. Rolandson, Lattice dynamics of copper at 80 K. *Phys. Rev. B* **7**, 2393-2400 (1973).
- [41] H. R. Schober, P. H. Dederichs, *Phonon states of elements. Electron states and Fermi surfaces of alloys. K.-H. Hellwege, J. L. Olsen (eds.)* (Springer-Verlag, Berlin, 1981).
- [42] J. W. Lynn, H. G. Smith, R. M. Nicklow, Lattice dynamics of gold. *Phys. Rev. B* **8**, 3493-3499 (1973).
- [43] G. Gilat, Phonon density of states in lead. *Solid State*

- Commun.* **3**, 101-103 (1965).
- [44] P. Söderlind, L. H. Yang, A. Landa, A. Wu, Mechanical and thermal properties for uranium and U-6Nb alloy from first-principles theory. *App. Sci.* **2021**, 5643 (2021).
- [45] M. E. Manley, A. H. Said, M. J. Fluss, M. Wall, J. C. Lashley, A. Alatas, K. T. Moore, Y. Shvyd'ko, Phonon density of states of  $\alpha$ - and  $\delta$ -plutonium by inelastic x-ray scattering. *Phys. Rev. B* **79**, 052301 (2009).
- [46] J. Wong, M. Krisch, D. L. Farber, F. Occelli, R. Xu, T.-C. Chiang, D. Clatterbuck, A. J. Schwartz, M. Wall, and C. Boro. Crystal dynamics of *d* fcc Pu-Ga alloy by high-resolution inelastic x-ray scattering. *Phys. Rev. B* **72**, 064115 (2005).
- [47] D. C. Wallace, Evaluation of thermodynamic functions of elemental crystals and liquids. *Phys. Rev. E* **56**, 1981-1986 (1997).
- [48] B. Lüthi, *Physical Acoustics in the Solid State* (Springer Berlin, Heidelberg 2005).
- [49] J. W. Arblaster, Thermodynamic Properties of Beryllium. *Journal of Phase Equilibria and Diffusion* **37**, 581-591 (2016). 2016
- [50] V. Y. Bodryakov, Joint studies of temperature dependences of thermal expansion and heat capacity of solid beryllium. *High Temperature* **56**, 185-192 (2018).
- [51] W. DeSorbo, Specific heat of diamond at low temperatures. *J. Chem. Phys.* **21**, 876-880 (1953).
- [52] A. C. Victor, Heat capacity of diamond at high temperature. *J. Chem. Phys.* **36**, 1903-1911 (1962).
- [53] M. Cardona, Albert Einstein as the father of solid state physics. preprint: arXiv:physics/0508237 (2005).
- [54] E. H. Buyco, F. E. Davis, Specific heat of aluminum from zero to its melting temperature and beyond. *J. Chem. Eng. Data* **15**, 518-523 (1970).
- [55] D. A. Ditmars, C. A. Plint, R. C. Shukla, Aluminum. I. Measurement of the relative enthalpy from 273 to 929 K and derivation of thermodynamic functions for Al(s) from 0 K to its melting point. *Int. J. Thermophys.* **6**, 499-515 (1985).
- [56] P. D. Desai, Thermodynamic properties of aluminum. *Int. J. Thermophys.* **8**, 621-638 (1987).
- [57] I. Barin, *Thermochemical Data of Pure Substances, 3rd ed.* (VCH Verlagsgesellschaft mbH: Weinheim, Germany, 1995).
- [58] K. C. Mills, *Recommended Values of Thermophysical Properties for Selected Commercial Alloys* (Woodhead Publishing Ltd.: Cambridge, UK, 2002).
- [59] M. W. Chase, NIST-JANAF Thermochemical Tables 4th ed. *J. Phys. Chem. Ref. Data Monogr.* **9**, 1-1951 (1998).
- [60] D. R. Lide, *The CRC Handbook of Chemistry and Physics, 90th Ed.* (internet version, CRC Press/Taylor and Francis, Boca Raton, Florida, 2009).
- [61] J. W. Arblaster, Thermodynamic Properties of Copper. *J. Phase. Equilib. Diff.* **36** 422 (2012).
- [62] K. Clusius, L. Schachinger, Ergebnisse der Tieftemperaturforschung. X Atomwärme des Indiums zwischen 12 und 273 K, *Z. Angew. Phys.* **4** 442-444 (1952).
- [63] J.R. Clement, E.H. Quinell, Atomic heat of indium below 20 K, *Phys. Rev.* **92**, 258-267 (1953).
- [64] W. Kramer, Nölting, Anomale Spezifische Wärmen und Fehlernung der Metalle Indium, Zinn, Blei, Zink, Antimon und Aluminium, *Acta* **20** 1353-1359 (1972).
- [65] F. Grønvold, Heat Capacity of indium form 300 to 1000K. *J. Therm. Anal.* **13** 419-428 (1978) .
- [66] V. A. Kirillin, A. E. Sheindlin, V. Y. Chekhovskoi, V. A. Petrov, Thermodynamic properties of tungsten in the temperature range of 0-3500 K. *Russ. J. Phys. Chem.* **37**, 2249-2256 (1963).
- [67] D. R. Stull, H. Prophet, *J. N. F. Thermochemical Tables, 2nd. ed.* (NBS, Washington, DC, 1971).
- [68] V. Y. Chekhovskoi, Enthalpy and heat caopacity of tungsten in the 400-3600 K temperature range. *Teplofizika Vysokikh Temperatur* **18**, 1191-1195 (1980).
- [69] V. Glushko, *Termodinamicheskie Svoistva Individual'nykh Veshchestv [Thermodynamic Properties of Individual Substances], 3rd ed.* (Nauka: Moscow, Russia, 1982); Volume 4, Book 2. (In Russian).
- [70] P. Gustafson, Evaluation of the thermodynamic properties of tungsten. *Int. J. Thermophys.* **6**, 395-409 (1985).
- [71] G. K. White, M. L. Minges, Thermophysical properties of some key solids: An update. *Int. J. Thermophys.* **18**, 1269-1327 (1997).
- [72] V. Y. Bodryakov, Correlation of temperature dependences of thermal expansion and heat capacity of refractory metal up to the melting point: Tungsten. *High Temp.* **53**, 643-648 (2015).
- [73] J. W. Arblaster, Thermodynamic properties of tungsten. *J. Phase Equilib. Diff.* **39**, 0689 (2018).
- [74] J. W. Arblaster, Thermodynamic properties of gold. *J. Phase Equilib. Diff.* **37**, 229-245 (2016).
- [75] Y. S. Touloukian, R. K. Kirby, R. E. Taylor, P. D. Desai, *Thermal Expansion, Thermophysical Properties of Matter, Vol. 12* (Plenum, New York, 1975).
- [76] I. Barin, O. Knacke, *Thermochemical Properties of Inorganic Substances* (Springer, Berlin, 1973).
- [77] Thermodynamic properties of lead. *CALPHAD* **39**, 47-53 (2012).
- [78] G. R. Stewart, Measurement of low-temperature specific heat. *Review of Scientific Instruments* **54**, 1-11 (1983).
- [79] V. Dremov, A. Karavaev, F. Sapozhnikov, M. Vorobyova, I Derbenev, L. Soulard, Molecular dynamic simulation of thermodynamic and mechanical properties and behaviour of Be when high rate straining. *DYMAT* **9**, 1277-1283 (2009).
- [80] E. S. Zouboulis, M. Grimsditch, A. K. Ramdas, S. Rodriguez, Temperature dependence of the elastic moduli of diamond: A Brillouin -scattering study. *Phys. Rev. B* **57**, 2889-2896 (1998).
- [81] A. Migliori, H. Ledbetter, R. G. Leisure, C. Pantea, J. B. Betts, Diamond's elastic stiffness from 322 K to 10 K. *J. Applied Phys.* **104**, 053512 (2008).
- [82] G. N. Kamm, G. A. Alers, Low-temperature elastic moduli of aluminum. *J. Applied Phys.* **35**, 327-330 (1964).
- [83] D. Gerlich, E. S. Fisher, The high temperature elastic moduli of aluminum. *J. Phys. Chem. Solids* **30**, 1197-1205 (1969).
- [84] W. C. Overton, J. Gaffney, Temperature variation of the elastic constants of cubic elements. I. Copper, *Phys. Rev.* **98**, 969-977 (1955).
- [85] Y. A. Chang, L. Himmel, Temperature dependence of elastic constants of Cu, Ag, and Au above room temperature. *J. Applied Phys.* **37**, 3567-3572 (1966).
- [86] B. S. Chandrasekhar, J. A. Rayne, Elastic constants of indium from 1.4° to 300°K. *Phys. Rev.* **124**, 1011-1014 (1961).
- [87] C. L. Vold, M. E. Glicksman, E. W. Kammer, L. C.



- Cardinal, Lead and indium from room temperature to the melting point. *J. Phys. Chem. Solids* **38**, 157-160 (1977).
- [88] R. Lowrie, A. M. Gonas, Single-crystal elastic properties of tungsten from 24° to 1800°C. *J. Applied. Phys.* **38**, 4505-4509 (1967).
- [89] J. R. Neighbours, G. A. Alers, Elastic constants of silver and gold. *Phys. Rev.* **111**, 707-712 (1958).
- [90] D. L. Waldorf, G. A. Alers, Low-temperature elastic moduli of lead. *J. Applied. Phys.* **33**, 3266-3269 (1962).
- [91] P. E. Armstrong, D. T. Eash, J. E. Hockett, Elastic moduli of alpha, beta and gamma polycrystalline uranium. *J. Nuclear Materials* **45**, 211-216 (1972/73).
- [92] F. J. Freibert, J. N. Mitchell, T. A. Saleh, A. Migliori *Instability and anharmonicity in plutonium thermo-physical properties* (Los Alamos National Laboratory, NM, 2012). <https://permalink.lanl.gov/object/tr?what=info:lanl-repo/lareport/LA-UR-12-22830>. Accessed 4 February 2020.
- [93] J. C. Lashley, B. E. Lang, J. Boerio-Goates, B. F. Woodfield, G. M. Schmiedeshoff, E. C. Gay, C. C. McPheeters, D. J. Thoma, W. L. Hults, J. C. Cooley, R. J. Hanrahan, Jr., and J. L. Smith, Low-temperature specific heat and critical magnetic field of  $\alpha$ -uranium single crystals. *Phys. Rev. B* **63**, 224510 (2001).
- [94] J. C. Lashley, J. Singleton, A. Migliori, J. B. Betts, R. A. Fisher, J. L. Smith, R. J. McQueeney, Experimental electronic heat capacities of  $\alpha$ - and  $\delta$ -plutonium: heavy fermion physics in an element. *Phys. Rev. Lett.* **91**, 205901 (2003).
- [95] A. C. Hewson, *The Kondo Problem to Heavy Fermions* (Cambridge University Press, Cambridge, 1993).
- [96] M. Wartenbe, P. H. Tobash, J. Singleton, L. E. Winter, S. Richmond, and N. Harrison, Pseudogap in elemental plutonium. *Phys. Rev. B* **105**, L041107 (2022).
- [97] A.C. Lawson, J.C. Lashley, Kondo entropy of  $\delta$ -phase plutonium and its impact on Pu alloy phase diagrams. *Phil. Mag.* **93**, 2377-2383 (2013).
- [98] J. A. Lee, P. W. Sutcliffe, K. Mendelssohn, Specific heat of  $\alpha$ -uranium. *Physics Letters* **30A**, 106-107 (1969).
- [99] J. Nakamjra, Y. Takahashi, S. Izumi, M. Kanno, Heat capacity of metallic uranium and thorium from 80 to 1000 K. *J. Nuclear Materials* **88**, 64-72 (1980).
- [100] J. C. Taylor, P. F. T. Linford, D. J. Dean, The low temperature elastic constants and specific heats of some  $\delta$ -phase plutonium-gallium alloys. *Institute of Metals Journal* **96**, 178-182 (1968).
- [101] J. E. Gordon, R. O. A. Hall, J. A. Lee, M. J. Mortimer, Heat capacities of plutonium and neptunium. *Proc. Roy. Soc. London A* **351**, 179-196 (1976).
- [102] S. S. Hecker, D. R. Harbur, T. G. Zocco, Phase stability and phase transitions in Pu-Ga alloys. *Prog. Mater. Science* **49**, 429-485 (2004).
- [103] K. D. Schotte and U. Schotte. Interpretation of Kondo experiments in a magnetic field. *Phys. Lett.* **55A**, 38-40 (1975).
- [104] W. P. Crummett, H. G. Smith, R. M. Nicklow, N. Wakabayashi, Lattice dynamics of  $\alpha$ -uranium. *Phys. Rev. B* **19**, 6028-6037 (1979).
- [105] R. A. Johnson, Analytic nearest-neighbor model for fcc metals. *Phys. Rev. B* **37**, 3924-3931 (1988).
- [106] D. G. Pettifor, Theoretical predictions of structure and related properties of intermetallics. *Mater. Sci. Technol.* **8**, 345-349 (1992).
- [107] M. E. Eberhart and T. E. Jones, Cauchy pressure and the generalized bonding model for nonmagnetic bcc transition metals. *Phys. Rev. B* **86**, 134106 (2012).
- [108] S. F. Pugh, XCII. Relations between the elastic moduli and the plastic properties of polycrystalline pure metals. *London Edinburgh Philos. Mag. & J. Sci.* **45**, 823-84 (1954).
- [109] D. G. Pettifor and M. Aoki, Bonding and Structure of Intermetallics: A New Bond Order Potential. *Philos. Trans. R. Soc. A* **334**, 439-449 (1991).
- [110] O. N. Senkov and D. B. Miracle, Generalization of intrinsic ductile-to-brittle criteria by Pugh and Pettifor for materials with a cubic crystal structure. *Sci. Rep.* **1**, 4531 (2021).
- [111] A. R. Organov, P. I. Dorogokupets, Intrinsic anharmonicity in equations of state and thermodynamics of solids. *J. Phys.: Condens. Matter* **16**, 1351-1360 (2004).
- [112] A. N. Filanovich, A. A. Povzner, Phonon anharmonicity and Gruneisen parameters of alpha-Plutonium, *J. Nuclear materials* **467**, 894-898 (2015).
- [113] A. Migliori, P. Söderlind, A. Landa, F. J. Freibert, B. Mayorov, B. J. Ramshaw, J. B. Betts, Origin of the multiple configurations that drive the response of  $\delta$ -plutonium's elastic moduli to temperature. *Proc. Nat. Acad. Sci. USA* **113**, 11158-11161 (2016).
- [114] N. Harrison, Electronically driven collapse of the bulk modulus in  $\delta$ -plutonium. *Proc. Nat. Acad. Sci. USA* **117**, 4480-4485 (2020).
- [115] S. P. Rudin, Symmetry-correct bonding in density functional theory calculations for delta phase Pu. *J. Nuc. Mat.* **570**, 153954 (2022).
- [116] P. S. Riseborough, X. Yang, Phonon anomalies in  $\alpha$ -uranium. *J. Magn. Mater.* **310**, 938-940 (2007).
- [117] P. Jacobson, S. Stoupin, Thermal expansion coefficient of diamond in a wide temperature range. *Diamond and Related Materials* **97**, 107469 (2019).
- [118] P. N. H. Nakashima, *The Crystallography of Aluminum and Its Alloys in Encyclopedia of Aluminum and Its Alloys; eds. George E. Totten, Murat Tiryakioğlu and Olaf Kessler* (CRC Press, Boca Raton, 2018), pp. 488-586.
- [119] N. V. Kozyrev, V. V. Gordeev, Thermodynamic equation of state for solid and liquid aluminum. *Metals* **12**, 1346 (2022).
- [120] N. V. Kozyrev, Thermodynamic properties and equation of state for solid and liquid copper. *International J. of Thermophysics* **44**, 31 (2023).
- [121] J. W. Arblaster, *Selected Values of the Crystallographic Properties of the Elements* (ASM International, Ohio, 2018).
- [122] N. V. Kozyrev, V. V. Gordeev, Thermodynamic properties and equation of state for tungsten. *Crystals* **13**, 1470 (2023).
- [123] M. G. Pamato, I. G. Wood, D. P. Dobson, S. A. Hunt, L. Vočadlo. *The thermal expansion of gold: point defect concentrations and pre-melting in a face-centred cubic metal. J. Appl. Cryst.* **51**, 470-480 (2018).
- [124] L. T. Lloyd, C. S. Barrett, Thermal expansion of alpha uranium. *J. Nuclear Materials* **18**, 55-59 (1966).
- [125] W. Voigt, *Lehrbuch der Kristallphysik* (Teubner, Leipzig, 1928), pp. 962.
- [126] A. J. Z. A. M. M. Reuss, Calculation of the flow limits of mixed crystals on the basis of the plasticity of monocrystals. *Z. Angew. Math. Mech.* **9**, 49-58 (1929).
- [127] R. Hill, Theory of Mechanical Properties of Fibre-

- strengthened Materials. 3. Self-consistent Model, *J. Mech. Phys. Solids* **13**, 189 (1965).
- [128] N. Harrison, J. B. Betts, M. R. Wartenbe, F. F. Balakirev, S. Richmond, M. Jaime, P. H. Tobash, Phase stabilization by electronic entropy in plutonium. *Nature Commun.* **10** 3159 (2019).
- [129] A. Tari, The heat capacity of matter at low temperatures (Imperial College Press, 1<sup>st</sup> ed., 2003).
- [130] S. K. Kushwaha, M. K. Chan, J. Park, S.M. Thomas, E. D. Bauer, J.D. Thompson, F. Ronning, P. F.S. Rosa and N. Harrison, Magnetic field-tuned Fermi liquid in a Kondo insulator. *Nat. Commun.* **10**, 5487 (2019).
- [131] J.-X. Zhu, R. C. Albers, K. Haule, G. Kotliar and J. M. Wills, Site-selective electronic correlation in  $\alpha$ -plutonium metal. *Nature Commun.* **4**, 2644 (2013).

#### ACKNOWLEDGEMENTS

Support was provided by Los Alamos National Laboratory LDRD project 20230042DR (code XXN0). A por-

tion of this work was carried out at the National High Magnetic Field Laboratory, which is funded by NSF Cooperative Agreement 1164477, the State of Florida and DoE.

#### AUTHOR CONTRIBUTIONS

#### COMPETING INTERESTS

The authors declare no competing interests.